

## High Performance Bianisotropic Metasurfaces: Asymmetric Transmission of Light

Carl Pfeiffer,<sup>1</sup> Cheng Zhang,<sup>1</sup> Vishva Ray,<sup>2</sup> L. Jay Guo,<sup>1</sup> and Anthony Grbic<sup>1,\*</sup>

<sup>1</sup>*Department of Electrical Engineering and Computer Science, University of Michigan, Ann Arbor, Michigan 48109-2122, USA*

<sup>2</sup>*Lurie Nanofabrication Facility, Department of Electrical Engineering and Computer Science, University of Michigan, Ann Arbor, Michigan 48109-2122, USA*

(Received 9 May 2014; published 10 July 2014)

It is experimentally shown that bianisotropic metasurfaces allow for extreme polarization control of light with high performance. A metasurface providing asymmetric transmission (i.e., polarization conversion) of circularly polarized light is reported at a wavelength of  $1.5\ \mu\text{m}$ . The experimental transmittance and extinction ratio are 50% and 20:1, which represents an order of magnitude improvement over previous optical structures exhibiting asymmetric transmission. The metasurface consists of patterned gold sheets that are spaced at a subwavelength distance from each other. The same design and fabrication processes can be used in the future to completely control the phase, amplitude, and polarization of light.

DOI: 10.1103/PhysRevLett.113.023902

PACS numbers: 42.25.Ja, 42.25.Bs, 78.67.Pt, 81.05.Xj

Controlling the polarization of light is critical to numerous optical systems [1]. Polarization control is typically achieved with combinations of linear polarizers and dielectric wave plates. However, these systems are bulky and do not lend themselves to nanophotonic system integration. Recently, metasurfaces have been introduced which allow polarization and wave front control across subwavelength thicknesses [2–4]. Metasurfaces are surfaces textured at a subwavelength scale to achieve tailored electromagnetic properties. They are the two-dimensional equivalent of metamaterials and have received much attention since they offer reduced losses, are lower profile, and are simpler to fabricate than bulk metamaterials [5].

A limited degree of polarization control can be achieved with metasurfaces that act as quarter-wave plates and half-wave plates [6–9]. However, more extreme polarization control requires low symmetry structures, for which systematic design methodologies have not been established [10,11]. As a result, their performance and impact on photonic systems have been limited. However, it was recently shown that bianisotropic metasurfaces composed of cascaded metallic sheets can be systematically designed to provide complete polarization control [12]. An experimental verification of the design methodology was performed at microwave frequencies [12]. Here, it is experimentally shown that high performance bianisotropic metasurfaces can be realized even at optical frequencies. An asymmetric circular polarizer that converts right-handed circularly polarized (RHCP) light into left-handed circularly polarized (LHCP) light is reported at a wavelength of  $1.5\ \mu\text{m}$ . The reported effect is similar to Faraday rotation but requires no magnetic field or nonreciprocal materials [13]. In addition, the device exhibits high polarization selectivity despite inherent losses. It transmits the circular polarization of one handedness and efficiently reflects the other, which is useful for a number of applications [14–16].

Consider two half-spaces (regions 1 and 2) separated by a metasurface at  $z = 0$ , as shown in Fig. 1. The fields in the two regions can be related through Jones calculus

$$\begin{pmatrix} E_t^x \\ E_t^y \end{pmatrix} = \begin{pmatrix} T_{xx} & T_{xy} \\ T_{yx} & T_{yy} \end{pmatrix} \begin{pmatrix} E_i^x \\ E_i^y \end{pmatrix} = \mathbf{T}_{\text{lin}} \begin{pmatrix} E_i^x \\ E_i^y \end{pmatrix}, \quad (1)$$

where  $\mathbf{T}$  is the Jones matrix of the metasurface, while  $E_i^{x,y}$  and  $E_t^{x,y}$  are the incident and transmitted fields, polarized in the  $x$  and  $y$  directions, respectively. The Jones matrix can also be written for circular polarization by replacing  $x$  and  $y$  bases with those for RHCP and LHCP. The idealized asymmetric circular polarizer considered here completely transmits right-handed circular polarization that is incident from region 1 but completely reflects right-handed circular polarization that is incident from region 2. It has the following Jones matrix in the linear and circular polarization bases [10]

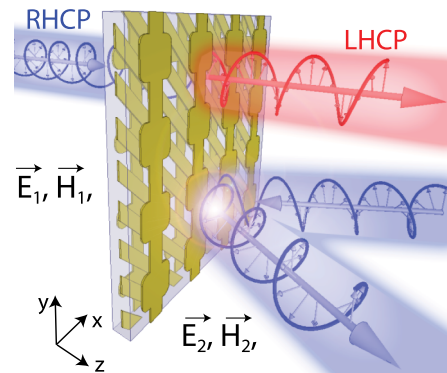


FIG. 1 (color online). An artistic rendering of the asymmetric circular polarizer converting right-handed circularly polarized light from region 1 to left-handed circularly polarized light in region 2. However, right-handed circularly polarized light is completely reflected when incident from region 2.

$$\mathbf{T}_{\text{lin}} = \frac{e^{j\phi}}{2} \begin{pmatrix} 1 & j \\ j & -1 \end{pmatrix}, \quad \mathbf{T}_{\text{circ}} = e^{j\phi} \begin{pmatrix} 0 & 0 \\ 1 & 0 \end{pmatrix}, \quad (2)$$

where  $\phi$  is an arbitrary phase shift through the metasurface and a time-harmonic progression of  $e^{j\omega t}$  is assumed. It should be noted that such a response does not violate reciprocity, and hence the performance of the structure can be analyzed by only considering plane waves incident from region 1 [10].

To date, the most common method of demonstrating asymmetric circular transmission is to employ structures with a purely electric response, such as printing two-dimensional chiral patterns on a single sheet [13,17]. In such a scheme, the asymmetric response is significant only when the eigenvectors of the sheet admittance (surface conductivity) are complex. This necessarily requires high loss, which fundamentally limits the efficiency of these structures. However, it was recently shown that an additional magnetic response is required to realize a high transmission and efficiency [12]. Specifically, the electric and magnetic responses need to be anisotropic. This can be realized using the geometry shown in Fig. 2. It consists of cascaded metallic sheets (electric sheet admittances) separated by substrates of a given intrinsic impedance ( $\eta_d$ ) and optical thickness ( $\beta d$ ) [16,18]. Each sheet is textured at a subwavelength scale to exhibit a specified anisotropy. This geometry is attractive because it allows metasurfaces to be straightforwardly designed and fabricated, even at optical

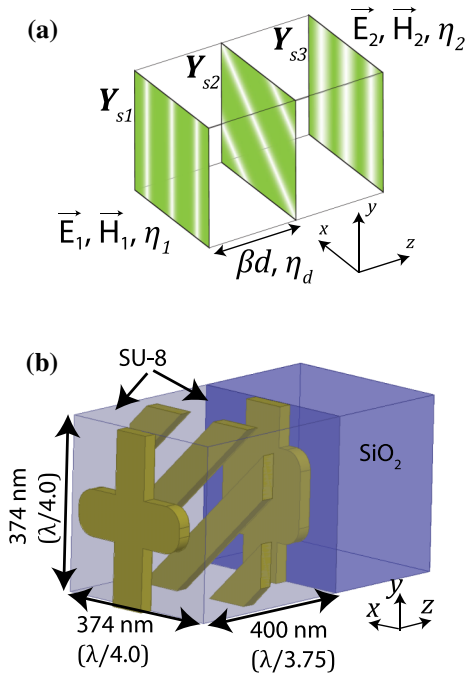


FIG. 2 (color online). Unit cell design. (a) Analytic model of a unit cell comprising the asymmetric circular polarizer. (b) Perspective view of the designed unit cell. Exact dimensions of the Au patterns are provided in the Supplemental Material [27].

wavelengths [19,20]. It should be emphasized that the cascaded structure can be modeled as a single bianisotropic metasurface, provided its overall thickness is subwavelength [12,21].

It was recently shown that a wide range of bianisotropic responses (e.g., polarization rotation, asymmetric circular transmission, asymmetric linear transmission, and symmetric circular transmission) can be systematically designed using the cascaded structure shown in Fig. 2. The design procedure is detailed in Ref. [12] and is highlighted here. We first note that the analytic model shown in Fig. 2(a) can be used to solve for the Jones matrix of the structure in terms of the cascaded sheet admittances [12]. However, we are looking to solve the inverse problem: to find the sheet admittances needed for a specified Jones matrix. This inverse problem is numerically solved using the FMINCON function provided by MATLAB's optimization toolbox. It was found that three anisotropic sheets were the minimum number required for a numerical solution. Once the required sheet admittances are known, their physical realization is straightforward. Typically, each sheet is independently designed by patterning gold (Au) on a dielectric substrate. Frequency-selective surface theory has provided extensive literature on realizing arbitrary electric sheet admittances [22]. It should be noted that patterning high permittivity dielectrics such as silicon is also an attractive option, since it promises reduced loss [23–26].

The  $\text{SiO}_2$  substrate is modeled as a lossless, infinite half-space with an index of refraction of  $n_{\text{SiO}_2} = 1.45$ . The index of refraction of the SU-8 is  $n_{\text{SU-8}} = 1.57$ . The relative permittivity of Au at near-infrared wavelengths is described by the Drude model  $\epsilon_{\text{Au}} = \epsilon_\infty - \omega_p^2 / (\omega^2 + j\omega\omega_c)$ , with  $\epsilon_\infty = 9.0$ ; the plasma frequency is  $\omega_p = 1.363 \times 10^{16}$  rad/s (8.97 eV), and the collision frequency is  $\omega_c = 3.60 \times 10^{14}$  rad/s (0.24 eV). This collision frequency assumes a loss that is over 3 times that of bulk Au [28], to take into account thin film surface scattering and grain boundary effects [29].

The patterns of each Au sheet are shown in Fig. 2(b), while detailed dimensions can be found in the Supplemental Material [27]. At the design wavelength of  $1.5 \mu\text{m}$ , the metallic patterns shown in Fig. 2(b) realize simulated sheet admittances of

$$\mathbf{Y}_{s1} = \frac{1}{\eta_0} \begin{pmatrix} 0.24 + 1.36j & 0 \\ 0 & 0.36 - 1.85j \end{pmatrix},$$

$$\mathbf{Y}_{s2} = \frac{1}{\eta_0} \begin{pmatrix} 1.01 - 2.87j & -0.98 + 3.67j \\ -0.98 + 3.67j & 1.01 - 2.87j \end{pmatrix},$$

and

$$\mathbf{Y}_{s3} = \frac{1}{\eta_0} \begin{pmatrix} 0.17 + 1.67j & 0 \\ 0 & 0.54 - 2.28j \end{pmatrix},$$

for the first, second, and third patterned Au sheets, respectively. All three sheets are inductive along one principal axis and capacitive along the orthogonal axis. In other words, each sheet has a continuous metallic trace along one principal axis and small gaps along the orthogonal axis. Using full-wave electromagnetic simulations, the width of each metallic trace and the size of the gap were designed such that the inductance and capacitance approached the ideal values that were numerically computed using the analytic model of Fig. 2(a). It should be noted that if material losses are neglected, the sheet admittances are purely imaginary. In this lossless case, the structure can provide 100% polarization conversion from RHCP to LHCP [12]. However, all metals exhibit loss at near-infrared wavelengths. This causes the sheet admittances to become complex, where the real part represents absorption in the metal. The loss reduced the efficiency of the metasurface to 53%.

It should be noted that it is possible to realize an asymmetric circular polarizer by cascading a quarter-wave plate, a linear polarizer, and another quarter-wave plate [30]. In fact, such a configuration provides some intuition on the operation of the metasurface shown in Fig. 2(b). Similar to a linear polarizer, the middle sheet reflects the majority of the power that is polarized along the  $(\hat{x} - \hat{y})/\sqrt{2}$  direction. Similar to a quarter-wave plate, the  $\hat{x}$  and  $\hat{y}$  polarizations experience different phase shifts when passing through the outer sheets. This analogy between each metallic sheet and a standard optical device does provide some physical intuition, but it is also overly

simplistic. Although the second sheet looks very similar to a wire grid polarizer, there are some important differences. Wire grid polarizers are generally designed to minimize the inductance along the wires while also minimizing the capacitance orthogonal to the wires in order to provide high reflection and transmission, respectively. In contrast, the cell size and patterned Au presented here are chosen to realize a specific capacitance  $[Y_{s2} = (0.03 + 0.82j)/\eta_0]$  along the  $(\hat{x} + \hat{y})/\sqrt{2}$  axis in order to achieve an optimal performance at the design wavelength. In addition, the outer sheets do not act as ideal quarter-wave plates since the transmitted phase difference between  $\hat{x}$  and  $\hat{y}$  polarizations is closer to  $60^\circ$  rather than the ideal  $90^\circ$ . Therefore, it should be emphasized that the metasurface has an operating principle that is fundamentally different from devices that achieve polarization control through cascading Jones matrices [30]. Each sheet of the metasurface shown in Fig. 2(b) provides significant reflection on its own. However, when all three sheets are cascaded together, the resulting interference generates high transmission of the desired polarization and high reflection of the undesired polarizations.

The metasurface is fabricated on a  $500 \mu\text{m}$  thick fused silica substrate using the process shown in Fig. 3(a) [19,20]. First, the bottom sheet admittance ( $Y_{s3}$ ) is fabricated by patterning a 2 nm Ti adhesion layer and a 28 nm Au layer using electron-beam lithography and liftoff with a Poly (methyl methacrylate) (PMMA) resist. Next, a 200 nm thick, SU-8 dielectric layer is spin coated onto the wafer, which naturally planarizes the surface for the following layer. This process is repeated until three Au layers are

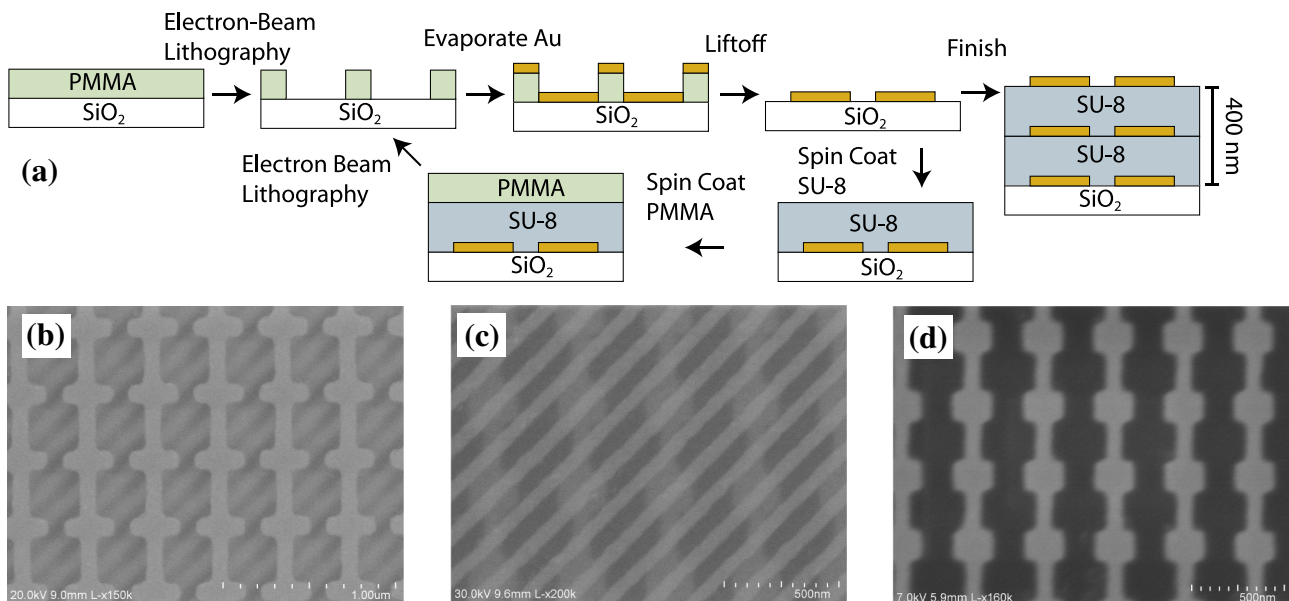


FIG. 3 (color online). Fabrication of the asymmetric circular polarizer. (a) Fabrication process involves sequential patterning of each 2 nm/28 nm thick Ti/Au layer using electron-beam lithography and liftoff, followed by spin coating of a 200 nm thick SU-8 dielectric layer. Three metallic layers are patterned using the process, resulting in an overall thickness of 430 nm. (b) SEM picture of the first Au sheet ( $Y_{s1}$ ). The second sheet can be seen below the first, although it is less clear. (c) SEM picture of the second Au sheet ( $Y_{s2}$ ). The third sheet can be seen below it. (d) SEM picture of the third Au sheet ( $Y_{s3}$ ).

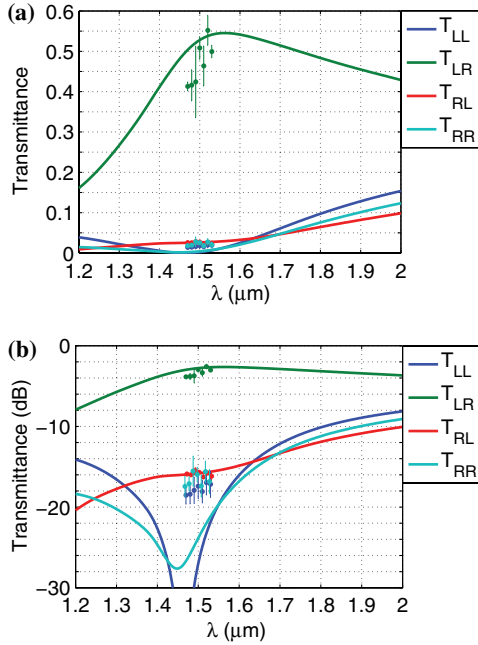


FIG. 4 (color online). Measured and simulated Jones matrix of the metasurface on (a) linear and (b) logarithmic scales. Solid lines correspond to simulation, whereas circles correspond to measurements. Error bars denote 1 standard deviation in the measured data. It can be seen that the metasurface provides high transmission of 50% for the left-handed circular when the right-handed circular is incident. In addition, all other elements of the Jones matrix in the circular polarization basis are below 2.5% at the operating wavelength of  $1.5 \mu\text{m}$ .

patterned to achieve the unit cell shown in Fig. 2(b). The patterned area is  $250 \times 250 \mu\text{m}$ . Scanning electron microscope (SEM) pictures of the three Au layers comprising the fabricated metasurface are shown in Figs. 3(b)–3(d). Additional details of the fabrication process are provided in the Supplemental Material [27]. In the future, large area soft lithography processes, such as nanoimprint lithography, can be employed to dramatically reduce the fabrication cost [31].

Following fabrication, the metasurface was experimentally characterized. The output of a  $1.5 \mu\text{m}$  tunable laser (Newport TLB 6326) was sent through a linear polarizer, followed by a quarter-wave plate, and then focused upon the metasurface. The transmitted power was collected by another quarter-wave plate, followed by a linear polarizer, and then received by a power meter. Rotating the quarter-wave plates allowed for characterization of the metasurface’s Jones matrix. The measured and simulated transmittance are plotted in Fig. 4 and show close agreement. At the operating wavelength of  $1.5 \mu\text{m}$ , the fabricated metasurface provides a high transmittance of 50% for left-handed circular polarization when right-handed circular polarization is incident. In addition, all other elements of the Jones matrix in the circular polarization basis are below 2.5%, which suggests an extinction ratio of

20:1. The extinction ratio is defined as the ratio of transmittance from RHCP to LHCP ( $T_{LR}$ ) relative to the maximum transmittance of RHCP to RHCP ( $T_{RR}$ ), LHCP to LHCP ( $T_{LL}$ ), and LHCP to RHCP ( $T_{RL}$ ). These experimental results represent an order of magnitude improvement in the extinction ratio over the state-of-the-art optical structures providing asymmetric transmission for both linear and circular polarizations [17,32–34]. This extinction ratio is comparable to that of the Au helix metamaterial, which acts as a symmetric circular polarizer [14]. However, the Au helix operates at longer wavelengths ( $3.5$  to  $7.5 \mu\text{m}$ ), requires a complex fabrication process (3D laser writing and gold plating), and its design cannot be extended to alternative polarization controlling devices. In contrast, the design and fabrication procedures presented here can realize a large range of bianisotropic metasurfaces such as symmetric circular polarizers, polarization rotators, and asymmetric linear polarizers by simply fabricating different metallic patterns [12].

Simulations indicate that when right-handed circular is incident, 37% of the power is absorbed in the Au patterns while 10% is reflected, thus resulting in a 53% efficiency. Alternatively, when left-handed circular is incident, 37% of the power is absorbed and 60% of the power is reflected (see the Supplemental Material [27]). The metasurface also has a robust angular tolerance due to the subwavelength cell size [35]. Only when the incident angle exceeds  $40^\circ$  does the performance begin to deteriorate, which is useful for many applications [36,37] (see the Supplemental Material [27]). It should also be noted that the angle of incidence is always identical to the angle of the transmitted wave for periodic metasurfaces with cell sizes less than  $\lambda/2$ , as is the case here. Figure 4 shows that the simulated response is quite broadband. However, the bandwidth of the available laser source limited measurements to the wavelength range of  $1.47$  to  $1.53 \mu\text{m}$ .

A metasurface providing asymmetric transmission of circularly polarized light is experimentally demonstrated. The simple design and fabrication process provides flexibility in realizing arbitrary bianisotropic metasurfaces that manipulate the polarization of light within a subwavelength thickness [12]. In the future, inhomogeneous metasurfaces will be developed that provide far greater phase and polarization control than the metasurfaces reported to date [38]. Thus, a single, ultrathin metasurface could replace bulky optical setups requiring combinations of conventional components such as lenses, spatial light modulators, wave plates, and linear polarizers.

The authors acknowledge helpful discussions with Dr. Nikolaos Limberopoulos and Dr. Boris Tomasic from the Sensors Directorate, Air Force Research Laboratory. This work was supported by the the Air Force Research Laboratory through the Advanced Materials, Manufacturing and Testing Information Analysis Center (AMMTIAC) Contract with Alion Science and

Technology, Contract No. FA4600-060D003, NSF Materials Research Science and Engineering Center (MRSEC) Program DMR 1120923, and a Presidential Early Career Award for Scientists and Engineers No. FA9550-09-1-0696. We acknowledge the technical support from the Lurie Nanofabrication Facility (LNF) at the University of Michigan. C. P. designed and simulated the metasurface under the supervision of A. G., and C. Z. fabricated the metasurface under the supervision of L. J. G. Both C. Z. and C. P. performed the measurements. V. R. provided extensive assistance in the electron-beam lithography. All authors contributed to the writing and editing of the manuscript. C. Pfeiffer and C. Zhang contributed equally to this work.

\*To whom all correspondence should be addressed.  
agrbc@umich.edu

- [1] Q. Zhan, *Adv. Opt. Photonics* **1**, 1 (2009).
- [2] A. V. Kildishev, A. Boltasseva, and V. M. Shalaev, *Science* **339**, 1232009 (2013).
- [3] A. Silva, F. Monticone, G. Castaldi, V. Galdi, A. Alù, and N. Engheta, *Science* **343**, 160 (2014).
- [4] N. Yu and F. Capasso, *Nat. Mater.* **13**, 139 (2014).
- [5] C. L. Holloway, E. F. Kuester, J. A. Gordon, J. O'Hara, J. Booth, and D. R. Smith, *IEEE Antennas Propag. Mag.* **54**, 10 (2012).
- [6] N. Yu, F. Aieta, P. Genevet, M. A. Kats, Z. Gaburro, and F. Capasso, *Nano Lett.* **12**, 6328 (2012).
- [7] M. Euler, V. Fusco, R. Cahill, and R. Dickie, *IEEE Trans. Antennas Propag.* **58**, 2457 (2010).
- [8] Y. Zhao and A. Alù, *Phys. Rev. B* **84**, 205428 (2011).
- [9] L. Cong, N. Xu, J. Gu, R. Singh, J. Han, and W. Zhang, *Laser Photonics Rev.* **8**, 626 (2014).
- [10] C. Menzel, C. Rockstuhl, and F. Lederer, *Phys. Rev. A* **82**, 053811 (2010).
- [11] T. Niemi, A. Karilainen, and S. Tretyakov, *IEEE Trans. Antennas Propag.* **61**, 3102 (2013).
- [12] C. Pfeiffer and A. Grbic, [arXiv:1404.3313](https://arxiv.org/abs/1404.3313).
- [13] V. A. Fedotov, P. L. Mladyonov, S. L. Prosvirnin, A. V. Rogacheva, Y. Chen, and N. I. Zheludev, *Phys. Rev. Lett.* **97**, 167401 (2006).
- [14] J. K. Gansel, M. Thiel, M. S. Rill, M. Decker, K. Bade, V. Saile, G. von Freymann, S. Linden, and M. Wegener, *Science* **325**, 1513 (2009).
- [15] Z. Y. Yang, M. Zhao, P. X. Lu, and Y. F. Lu, *Opt. Lett.* **35**, 2588 (2010).
- [16] Y. Zhao, M. A. Belkin, and A. Alù, *Nat. Commun.* **3**, 870 (2012).
- [17] A. S. Schwanecke, V. A. Fedotov, V. V. Khardikov, S. L. Prosvirnin, Y. Chen, and N. I. Zheludev, *Nano Lett.* **8**, 2940 (2008).
- [18] N. K. Grady, J. E. Heyes, D. R. Chowdhury, Y. Zeng, M. T. Reiten, A. K. Azad, A. J. Taylor, D. A. R. Dalvit, and H. Chen, *Science* **340**, 1304 (2013).
- [19] N. Liu, H. Guo, L. Fu, S. Kaiser, H. Schweizer, and H. Giessen, *Nat. Mater.* **7**, 31 (2008).
- [20] C. Pfeiffer, N. K. Emani, A. M. Shaltout, A. Boltasseva, V. M. Shalaev, and A. Grbic, *Nano Lett.* **14**, 2491 (2014).
- [21] C. L. Holloway, A. Dienstfrey, E. F. Kuester, J. F. O'Hara, A. K. Azad, and A. J. Taylor, *Metamaterials* **3**, 100 (2009).
- [22] B. A. Munk, *Frequency Selective Surfaces: Theory and Design* (Wiley, New York, 2005).
- [23] F. Monticone, N. M. Estakhri, and A. Alù, *Phys. Rev. Lett.* **110**, 203903 (2013).
- [24] C. Wu, N. Arju, G. Kelp, J. A. Fan, J. Dominguez, E. Gonzales, E. Tutuc, I. Brener, and G. Shvets, *Nat. Commun.* **5**, 3892 (2014).
- [25] Y. Yang, W. Wang, P. Moitra, I. I. Kravchenko, D. P. Briggs, and J. Valentine, *Nano Lett.* **14**, 1394 (2014).
- [26] Z. Bomzon, G. Biener, V. Kleiner, and E. Hasman, *Opt. Lett.* **27**, 285 (2002).
- [27] See Supplemental Material at <http://link.aps.org/supplemental/10.1103/PhysRevLett.113.023902> for additional information on the fabrication, design, and characterization of the metasurface.
- [28] P. B. Johnson and R. W. Christy, *Phys. Rev. B* **6**, 4370 (1972).
- [29] K. Chen, V. P. Drachev, J. D. Borneman, A. V. Kildishev, and V. M. Shalaev, *Nano Lett.* **10**, 916 (2010).
- [30] J. E. Roy and L. Shafai, *IEEE Antennas Propag. Mag.* **38**, 18 (1996).
- [31] L. Jay Guo, *Adv. Mater.* **19**, 495 (2007).
- [32] V. A. Fedotov, A. S. Schwanecke, N. I. Zheludev, V. V. Khardikov, and S. L. Prosvirnin, *Nano Lett.* **7**, 1996 (2007).
- [33] C. Menzel, C. Helgert, C. Rockstuhl, E. B. Kley, A. Tünnermann, T. Pertsch, and F. Lederer, *Phys. Rev. Lett.* **104**, 253902 (2010).
- [34] M. Mutlu, A. E. Akosman, A. E. Serebryannikov, and E. Ozbay, *Phys. Rev. Lett.* **108**, 213905 (2012).
- [35] M. A. Al-Joumayly and N. Behdad, *IEEE Trans. Antennas Propag.* **59**, 4542 (2011).
- [36] Y. J. Shin, Y.-K. Wu, K.-T. Lee, J. G. Ok, and L. J. Guo, *Adv. Opt. Mater.* **1**, 863 (2013).
- [37] Y.-K. R. Wu, A. E. Hollowell, C. Zhang, and L. J. Guo, *Sci. Rep.* **3**, 1194 (2013).
- [38] J. Lin, P. Genevet, M. A. Kats, N. Antoniou, and F. Capasso, *Nano Lett.* **13**, 4269 (2013).